# Progress Towards a Comprehensive Model for Mass Transfer in Structured Packings

Brian Hanley[1] and Jack Wilfert[1]

[1]Louisiana State University

May 15, 2023

I&EC research
Industrial & Engineering Chemistry Research

pubs.acs.org/IECR

Article

# Progress Toward a Comprehensive Model for Mass Transfer in Structured Packings

Jack Wilfert and Brian F. Hanley*

Cite This: https://doi.org/10.1021/acs.iecr.3c00769

Read Online

ACCESS | Metrics & More | Article Recommendations | Supporting Information

**ABSTRACT:** Significant effort has been devoted to the study of mass transfer in sheet metal structured packings over the past half century. A number of mass transfer correlations have appeared in the literature as a result of those efforts. Unfortunately, none of these correlations has shown itself to be reliable over the full range of chemical systems, column operating conditions, and packing topologies encountered today. In an attempt to rectify some of the shortcomings of earlier correlations for sheet metal structured packings, we have employed a new data analysis methodology which simultaneously fits ⟨HETP⟩ data and mass transfer area data. The correlation we report upon here includes 444 ⟨HETP⟩ values from a variety of systems, operating pressures, and packing designs, along with 409 mass transfer area measurements. We demonstrate that this correlation outperforms all others while remaining simple enough to implement in process simulation software.

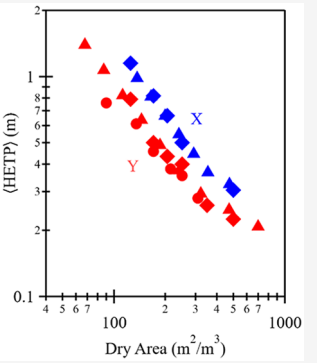




## INTRODUCTION

Sheet metal structured packing ⟨HETP⟩ values for binary systems measured at total reflux are surprisingly well-described by simple expressions like the correlation of Harrison and France and Kister for "Y" style structured packings.[1−11] Those relationships between ⟨HETP⟩ and dry packing surface area per unit volume have been found to predict ⟨HETP⟩ values to within ±30% on average regardless of system, column pressure, and details of the surface topology of the packing. Other slightly more complex rules yield ⟨HETP⟩ estimates with somewhat improved levels of uncertainty.[12−14] Cmelíková et al. discuss the aforementioned findings in-depth.[15] Figure 1 is a parity plot of the Carillo and Harrison and France estimating rules applied to our data set.[11,13]

Mass transfer correlations for structured packings based on the two-resistance concept, usually coupled with some appeal to penetration theory, the Chilton-Colburn analogy, or surface renewal theory, often outperform the rules-of-thumb described above for specific systems and packing sizes but usually perform relatively poorly when used outside of their original correlating data sets.[16−22] Figure 2 is a parity plot of modeled versus experimental ⟨HETP⟩s for the correlations of Harrison and France, Bravo et al., Hanley and Chen, and Wang et al. for our data set.[11,17,19,20]

Table 1 details the physical and transport property ranges for our data set. Included are recent efficiency measurements taken by Bradtmöller and Scholl on the system 2-methyl-2-butanol/2-methyl-1-propanol at or below atmospheric pressure.[3] Clearly this system, under these conditions, has a noticeably higher liquid viscosity (and consequently lower liquid phase diffusivity) than the other standard distillation test

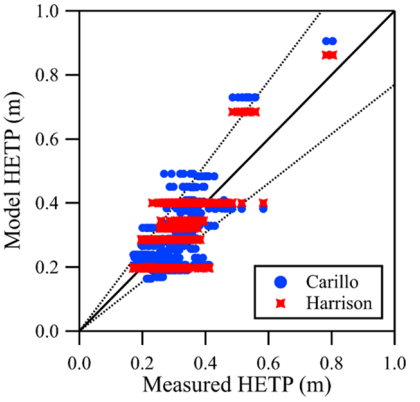


**Figure 1.** Parity plot of ⟨HETP⟩ predictions from the Carillo and Harrison and France estimating rules versus measured ⟨HETP⟩ values. Dotted lines are ±20% around the diagonal.

mixtures in the data set. The addition of these high liquid viscosity and low liquid diffusivity experiments exposes the fact that current mass transfer correlations have too strong a dependence on physical properties. One of the goals of this paper is to develop a mass transfer correlation that weakens these extraneous physical property effects.

**Received:** March 9, 2023
**Revised:** April 28, 2023
**Accepted:** May 2, 2023

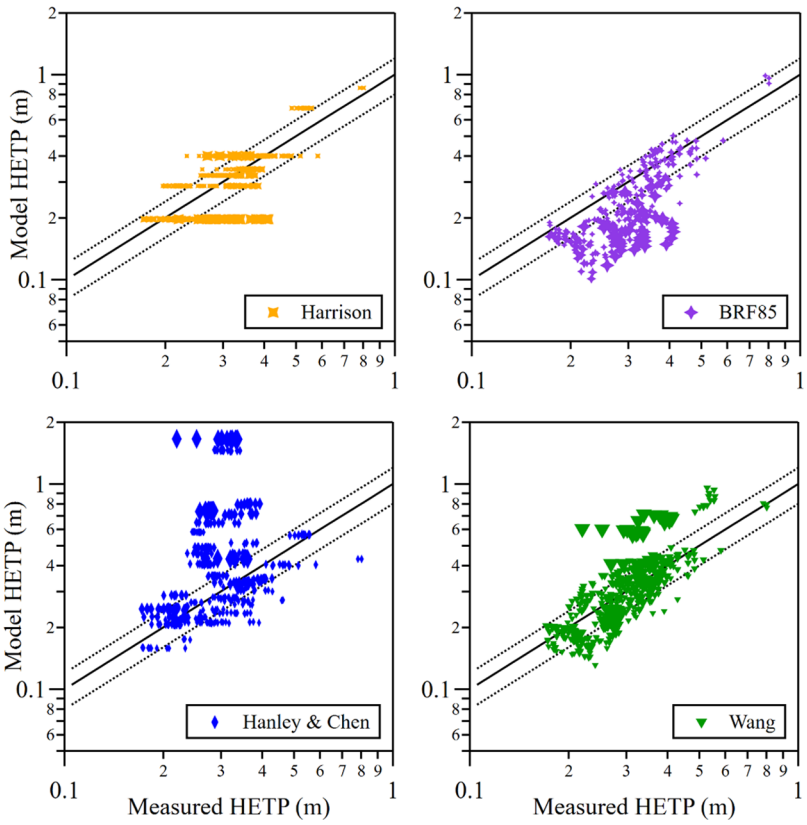


**Figure 2.** Parity plots of modeled ⟨HETP⟩ versus measured ⟨HETP⟩ for three different mass transfer correlations along with a similar parity plot for the estimating rule of Harrison and France. Dotted lines are ±20% around the diagonal.

**Table 1. Summary of Estimated Physical Property Data Ranges for the ⟨HETP⟩ Data in the Regression Data Set[a]**

| | With Bradmoller data | | | Without Bradmoller data | | |
|---|---|---|---|---|---|---|
| Property | Max | Min | Range | Max | Min | Range |
| $\rho_L$ (kg/m$^3$) | 1129.63 | 487.21 | 2.32 | 1129.63 | 487.21 | 2.32 |
| $\rho_V$ (kg/m$^3$) | 28.25 | $6.66 \times 10^{-02}$ | 424.3 | 28.25 | $8.25 \times 10^{-02}$ | 342.6 |
| $D_L$ (m$^2$/sec) | $1.18 \times 10^{-08}$ | $3.59 \times 10^{-10}$ | 32.84 | $1.18 \times 10^{-08}$ | $2.09 \times 10^{-09}$ | 5.64 |
| $D_V$ (m$^2$/sec) | $1.55 \times 10^{-04}$ | $5.75 \times 10^{-07}$ | 269.7 | $1.15 \times 10^{-04}$ | $5.75 \times 10^{-07}$ | 200.7 |
| $\sigma_L$ (N/m) | $2.99 \times 10^{-02}$ | $5.22 \times 10^{-03}$ | 5.71 | $2.74 \times 10^{-02}$ | $5.22 \times 10^{-03}$ | 5.25 |
| $\mu_L$ (Pa-sec) | $3.27 \times 10^{-03}$ | $9.21 \times 10^{-05}$ | 35.52 | $5.85 \times 10^{-04}$ | $9.21 \times 10^{-05}$ | 6.35 |

[a]Properties were estimated with Aspen Properties V11. For the systems $iC_4/nC_4$ and $Ar/O_2$, the REFPROP property method was used; the UNIFAC property method was employed for the systems p-xylene/o-xylene, cyclohexane/*n*-heptane, chlorobenzene/ethylbenzene, 2-methyl-2-butanol/2-methyl-1-propanol, and i-octane/toluene.

Additionally, as carbon capture via absorption in packed towers becomes increasingly important, we demonstrate that the mass transfer correlation developed in this work can be used to quantitatively match important experimental results when implemented in rate-based carbon capture simulations.[23−26]

## PRELIMINARIES

We have chosen to use dimensionless power law expressions to correlate our data because they are relatively simple to implement, they have been used to correlate mass and heat transfer phenomena effectively, and because certain process simulators have the ability to use general power law expressions for the mass transfer coefficients and interfacial area in rate-based simulations.[27−30] Eq 1 through eq 6 define the structure and the 12 fitting coefficients needed to completely define our correlation.

$$Sh_V = C_1 \mathrm{Re}_V^{C_2} Sc_V^{C_3} \left( \frac{\cos(\theta)}{\cos(\pi/4)} \right)^{C_4} \tag{1}$$

$$Sh_L = C_5 \mathrm{Re}_L^{C_6} Sc_L^{C_7} \left( \frac{\cos(\theta)}{\cos(\pi/4)} \right)^{C_8} \tag{2}$$

$$\frac{a_m}{a_d} = C_9 \mathrm{Re}_V^{C_{10}} We_L^{C_{11}} Fr_L^{C_{12}} \tag{3}$$

$$Sh_V = \frac{k_y d_e}{c_V \mathcal{D}_V} \tag{4}$$

$$Sh_L = \frac{k_x d_e}{c_L \mathcal{D}_L} \tag{5}$$



https://doi.org/10.1021/acs.iecr.3c00769
Ind. Eng. Chem. Res. XXXX, XXX, XXX−XXX

$$d_e = \frac{4\epsilon}{a_d} \tag{6}$$

$$\langle \mathrm{HETP} \rangle = \frac{G}{a_m}\left(\frac{C_y}{k_y} + \frac{C_x}{k_x}\right) \tag{7}$$

The ⟨HETP⟩ values in our data set were all taken at total reflux. Figure 3 demonstrates that the vapor and liquid phase

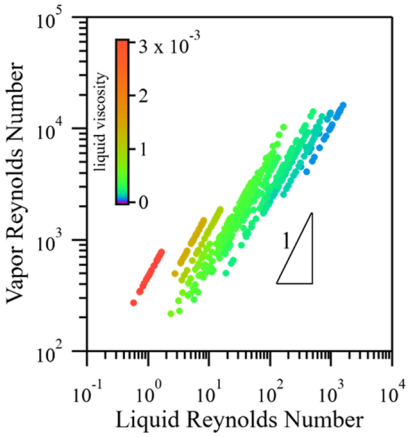


**Figure 3.** Vapor phase Reynolds number versus liquid phase Reynolds number for the efficiency experiments analyzed for this paper. All of these experiments were performed at total reflux. This leads to a high degree of correlation between these two dimensionless groups, which creates statistical difficulties with regard to deconvoluting liquid effects from vapor effects. Data points are colored by liquid viscosity in Pa-sec.

Reynolds numbers are highly correlated for these types of experiments, and this leads to large statistical uncertainties in the values of multiple fitted coefficients in the expressions above. In order to bypass some of the ambiguity introduced into the fitting process by this high level of correlation between two important dimensionless groups, the developers of past correlations have often fixed the powers on the Reynolds and Schmidt numbers in eq 1 and eq 2 to be in agreement with theoretically expected values from one of the models for mass transfer mentioned earlier.

The dependence of the Sherwood number on the Reynolds and Schmidt numbers is widely accepted. The choice of dimensionless groups against which to correlate the interfacial area is much more open to speculation. We chose to use the liquid phase Froude ($Fr_L$) and Weber ($We_L$) numbers based primarily on the analysis provided by Tsai.[9] We added the vapor phase Reynolds number ($Re_V$) dependence to improve the fits.

As already mentioned, fixing the power law exponents $C_2$, $C_3$, $C_6$, and $C_7$ on the Reynolds and Schmidt numbers in eq 1 and eq 2 from available theories for mass transfer leads to unwanted residual physical and transport property effects that undermine the extensibility of these correlating expressions to systems outside of those included in the original data set. It is clear, therefore, that $C_2$, $C_3$, $C_6$, and $C_7$ cannot be set a priori. However, the statistical dilemma mentioned earlier directly undermines any attempt to regress these values cleanly from total reflux experimental data alone. This obstacle is compounded by the fact that the mass transfer area always appears in combination with the individual mass transfer coefficients. To simultaneously remove the statistical uncertainties inherent in total reflux experiments while allowing the power law coefficients $C_2$, $C_3$, $C_6$, and $C_7$ to float in the regression clearly requires other independent sources of data beyond the ⟨HETP⟩. We have therefore included Tsai's interfacial mass transfer area experiments on structured packings in our data set.[9] These experiments help to deconvolute the aforementioned statistical difficulties that arise from total reflux experiments and also help to isolate the calculation of the interfacial area in the products $k_x a_m$ and $k_y a_m$. Other researchers have also measured the interfacial area participating in mass transfer for structured packings.[31,32]

## DATA ANALYSIS

**Preliminaries.** Our data set included 444 individual ⟨HETP⟩ points for a variety of chemical systems and packing styles. The majority were collected by digitizing graphs from the various literature sources we used. Additionally, we recorded auxiliary experimental information, such as packing height and top/bottom compositions, when available.

Physical and transport property values were calculated from the Aspen Properties V11 add-in for Excel. The REFPROP property method was used for $iC_4/nC_4$ and $Ar/O_2$. This method is considered the most accurate for light hydrocarbon and small molecule mixtures.[33] For the remaining systems—p-xylene/o-xylene, cyclohexane/*n*-heptane, chlorobenzene/ethylbenzene, 2-methyl-2-butanol/2-methyl-1-propanol, and i-octane/toluene—we used the UNIFAC method. Representative thermodynamic and transport properties for the liquid phase were calculated for 50/50 mixtures at the bubble point for the reported nominal column pressure. Properties for the vapor phase were calculated at the vapor composition in equilibrium with the 50/50 liquid mix. In addition, all of the test systems in our data set have nearly constant relative volatilities. Typical $\alpha$ values could be calculated from the flash calculations just described. Physical properties calculated using a 50/50 mixture should produce representative average property values for most experimental distillations.

Liquid phase binary diffusivities did not come directly from the Aspen Properties add-in since it does not have a facility for returning a liquid phase binary diffusivity. Instead, it returns both tracer diffusivities for the binary mixture. Binary liquid diffusivities were therefore calculated via the method of Vignes (see eq 8), which includes a thermodynamic factor, $\beta$ (see eq 9), to represent solution nonideality.[34] This derivative was estimated numerically at equimolar compositions for each system, and in almost every case, the value approached 1.

$$\mathcal{D}_L = [(D^{\circ}_{AB})^{(1-x)}(D^{\circ}_{BA})^{x}]\beta \tag{8}$$

$$\beta = \frac{\partial \ln(a)}{\partial \ln(x)} \tag{9}$$

$C_x$ and $C_y$ are approximate weighting factors used to convert an array of point HETPs to ⟨HETP⟩ for the column. The derivation of these factors is described by Hanley and Chen in detail.[19] Typically, both values approach unity when top/bottom product compositions are far enough apart.

Additionally, our data set included 409 interfacial mass transfer area values and information about liquid and vapor flow rates from Tsai.[9] We supplemented these measurements with transport and physical property data for water under the


https://doi.org/10.1021/acs.iecr.3c00769
Ind. Eng. Chem. Res. XXXX, XXX, XXX−XXX

reported experimental conditions using the STEAM-TA Aspen Properties method.

**Nonlinear Regression.** Our complete data set thus consists of two independent subsets—the first ⟨HETP⟩-related and the second mass transfer area-related. The defining expressions that we plan to use to regress the entire data set require a software package with specific capabilities: 1) the ability to define arbitrary, complex target functions, 2) robust fitting algorithm(s), and 3) an associated programming language. We found that Igor Pro V9 satisfied all of these requirements.[35]

Our initial attempt at regression involved a simple substitution of eq 1 through eq 5 into eq 7 for the ⟨HETP⟩ with this expression to be used for data points 1 through 444,

$$\langle \mathrm{HETP} \rangle = \frac{G}{a_d C_9 \mathrm{Re}_V^{C_{10}} We_L^{C_{11}} Fr_L^{C_{12}}} \left( \frac{C_y}{C_1 \mathrm{Re}_V^{C_2} Sc_V^{C_3} \left( \frac{\cos(\theta)}{\cos(\pi/4)} \right)^{C_4} \left( \frac{c_V \mathcal{D}_V}{d_e} \right)} + \frac{C_x}{C_5 \mathrm{Re}_L^{C_6} Sc_L^{C_7} \left( \frac{\cos(\theta)}{\cos(\pi/4)} \right)^{C_8} \left( \frac{c_L \mathcal{D}_L}{d_e} \right)} \right) \tag{10}$$

while eq 3 would then be used directly for the remaining mass transfer area measurements. We used an "if" statement in our code to switch from one correlating expression to the other. Eq 10 was badly behaved during regression attempts. After several bids at reconfiguring this equation, we found that eq 11 below worked well.

$$\frac{\langle \mathrm{HETP} \rangle \left( \frac{c_V \mathcal{D}_V}{d_e} \right) \left( \frac{c_L \mathcal{D}_L}{d_e} \right) a_d}{G} = \frac{C_5 C_y \left( \frac{\cos(\theta)}{\cos(\pi/4)} \right)^{C_8} \mathrm{Re}_L^{C_6} Sc_L^{C_7} \left( \frac{c_L \mathcal{D}_L}{d_e} \right) + C_1 C_x \left( \frac{\cos(\theta)}{\cos(\pi/4)} \right)^{C_4} \mathrm{Re}_V^{C_2} Sc_V^{C_3} \left( \frac{c_V \mathcal{D}_V}{d_e} \right)}{C_1 C_5 C_9 Fr_L^{C_{11}} \mathrm{Re}_L^{C_6} Sc_L^{C_7} Sc_V^{C_3} We_L^{C_{12}} \left( \frac{\cos(\theta)}{\cos(\pi/4)} \right)^{(C_4+C_8)} \mathrm{Re}_V^{(C_2+C_{10})}} \tag{11}$$

Note that several known quantities and groupings have been transferred from the right-hand side of eq 11 to the left.

In addition, we imposed several constraints on the fitting coefficients.

$$C_{11} + C_{12} \geq 0$$

$$0 \leq C_2, C_3, C_6, C_7 \leq 1$$

The first constraint was included so that the mass transfer area increases with increasing liquid rate. The second set of constraints was imposed because the exponents on the Reynolds and Schmidt numbers in the mass transfer coefficient definitions are expected to be positive but not to exceed unity. This last condition was imposed because no current theory or model for mass transfer that we are aware of predicts exponents greater than one.

The values of the new dependent variable on the left-hand side of eq 11

$$\frac{\langle \mathrm{HETP} \rangle \left( \frac{c_V \mathcal{D}_V}{d_e} \right) \left( \frac{c_L \mathcal{D}_L}{d_e} \right) a_d}{G} \tag{12}$$

are several orders of magnitude smaller than typical values for the mass transfer area. In order to prevent the regression algorithm from weighting the mass transfer area values too highly, we fit the natural logarithm of eq 11 rather than eq 11 directly along with the mass transfer area data.

Eq 11 sheds some light on a few of the statistical difficulties inherent in trying to regress all 12 fitting coefficients using total reflux ⟨HETP⟩ data only. First, note that the front factors $C_1$, $C_5$, and $C_9$ in eq 1, eq 2, and eq 3 appear as a product in the denominator. While $C_1$ and $C_5$ appear independently in the numerator, it is nearly impossible to deconvolute these three coefficients with a satisfactory level of statistical confidence based entirely on total reflux ⟨HETP⟩ data. Inclusion of mass transfer area measurements along with ⟨HETP⟩ data greatly assists the regression algorithm's attempts to arrive at reproducible values for $C_1$, $C_5$, and $C_9$ with much reduced statistical uncertainty.

Additionally, the power law exponents $C_2$ and $C_6$ for the Reynolds numbers in eq 1 and eq 2 appear in both the numerator and the denominator. Figure 3 demonstrated that total reflux experiments yield highly correlated Reynolds numbers in the liquid and vapor phases. Consequently, the power law exponents $C_2$ and $C_6$ can be subject to substantial statistical uncertainty whenever the majority of the ⟨HETP⟩ data have been derived from total reflux experiments, even with the addition of the independent mass transfer area measurements. The uncertainty can be overcome, of course, if the value(s) of one or both exponents can be fixed so that they are excluded from the regression.

We noted earlier in passing that past mass transfer correlations for structured packings suffer some level of failure when used to predict ⟨HETP⟩ values because they are too strongly reliant upon individual phase thermodynamic and transport properties relative to what is observed experimentally. Virtually all property related effects on the ⟨HETP⟩ are removed when $C_2$, $C_3$, $C_6$, and $C_7$ are equal to one. We see then that

$$k_y = C_1 c_V \mathrm{v}_V \tag{13}$$

$$k_x = C_5 c_L \mathrm{v}_L \tag{14}$$

A slight residual property effect remains due to the appearance of $\rho_L$ and $\sigma_L$ in the Weber number, which appears in eq 3, but the effect is minor because these quantities appear together as $(\rho_L/\sigma_L)$ which effectively cancels most of their temperature/pressure dependence. We therefore anticipate that $C_2$, $C_3$, $C_6$, and $C_7$ should be close to one.

A regular part of the fitting procedure involved putting sets of regressed coefficients into Aspen Plus V11 on the generalized transport correlations page so that we could test ease of use for rate-based distillation calculations. These tests included, in particular, simulations of the carbon capture experiments of Notz et al.[23] The tests revealed that Aspen rate-based distillation would often struggle to converge or not converge at all with the coefficient set being tested. Failures



https://doi.org/10.1021/acs.iecr.3c00769
Ind. Eng. Chem. Res. XXXX, XXX, XXX−XXX

Table 2. A History of Regressed Values for the 12 Fitting Coefficients of Eq 1, Eq 2, and Eq 3 along with the Constraints Imposed for Each Regression

| | Regression 1 | Regression 2 | Regression 3 |
|---|---|---|---|
| $C_1$ | 0.03963 ± 0.0239 | 0.033324 ± 0.021 | 0.047431 ± 0.00614 |
| $C_2$ | 1 ± 0.0758 | 1 ± 0.0759 | 1 ± 0 |
| $C_3$ | 1 ± 0.379 | 1 ± 0.291 | 1 ± 0 |
| $C_4$ | 0.78687 ± 0.441 | 0.55209 ± 0.422 | 1.0167 ± 0.488 |
| $C_5$ | 0.19142 ± 0.128 | 0.16662 ± 0.127 | 0.16723 ± 0.00958 |
| $C_6$ | 0.75277 ± 0.0528 | 0.8 ± 0.0625 | 0.75 ± 0 |
| $C_7$ | 0.73965 ± 0.0522 | 0.75821 ± 0.0602 | 0.75 ± 0 |
| $C_8$ | 0.62274 ± 0.245 | 0.74722 ± 0.289 | 0.53775 ± 0.221 |
| $C_9$ | 0.68195 ± 0.0552 | 0.80933 ± 0.0659 | 0.63149 ± 0.0395 |
| $C_{10}$ | 0.0026523 ± 0.0134 | −0.029328 ± 0.0136 | 0.016881 ± 0.00955 |
| $C_{11}$ | 0.17096 ± 0.00787 | 0.17537 ± 0.00793 | 0.16898 ± 0.00737 |
| $C_{12}$ | −0.11282 ± 0.00763 | −0.12084 ± 0.00768 | −0.10929 ± 0.00697 |
| | | Constraints | |
| | $0 \le C_2 \le 1$ | $0 \le C_2 \le 1$ | $C_2 = 1$ |
| | $0 \le C_3 \le 1$ | $0 \le C_3 \le 1$ | $C_3 = 1$ |
| | $0 \le C_6 \le 1$ | $0 \le C_6 \le 1$ | $C_6 = 0.75$ |
| | $0 \le C_7 \le 1$ | $0 \le C_7 \le 1$ | $C_7 = 0.75$ |
| | $C_{11} + C_{12} \ge 0$ | $C_{11} + C_{12} \ge 0$ | $C_{11} + C_{12} \ge 0$ |
| | | $C_5 = 5\ C_1$ | |

most often occurred at the stripper. This behavior, then, imposed another constraint on our fitting procedure. The test simulations using rate-based calculations in Aspen Plus created a paradoxical situation: sets of coefficients that would be statistically "optimal" in some sense were not, however, optimal in the sense of "usability" for process simulation. Given the number of coefficients, the complexity of rate-based calculations in general, and our lack of access to Aspen's source code, we found this usability issue hard to address in any systematized way. In the end, we would impose what we considered to be reasonable constraints on some coefficients, fix others, and then use the resultant fitted coefficient set in a few rate-based simulations that would always include the simulations of the carbon-capture pilot tests of Notz. If the coefficient set required extreme efforts to get even one of these simulations to converge, or if even one simulation could not be converged, then we would refit the data set using different constraints/assumptions.

Three sets of regression coefficients are listed in Table 2 along with their estimated uncertainties (as standard deviations) and the constraints applied to the fitting procedure to obtain them. Note that the uncertainties in $C_1$ and $C_5$, the front factors on the power law expressions for the Sherwood numbers (see eq 1 and eq 2), are exceptionally large for regression 1 and regression 2, primarily due to the statistical difficulties that result from having all ⟨HETP⟩ data taken at total reflux. Note also that the power law exponents on the vapor phase Reynolds and Schmidt numbers for regression 1 and regression 2 ($C_2$ and $C_3$) tend to settle at one, while those same power law exponents on the liquid phase Reynolds and Schmidt numbers ($C_6$ and $C_7$) settle near 0.75. We used this behavior in regression 3 by fixing $C_2$ and $C_3$ at 1 and $C_6$ and $C_7$ at 0.75. Fixing the power law exponents resolves most of the statistical cross-effects inherent in total reflux experiments and thus greatly reduces the uncertainties in the front factors $C_1$ and $C_5$. We consider regression 3 the best statistical fit and also the best fit for use on the generalized mass transfer coefficient input page of Aspen Plus. The final correlating expressions thus become

$$Sh_V = 0.0474\mathrm{Re}_V^{1} Sc_V^{1}\left(\frac{\cos(\theta)}{\cos(\pi/4)}\right)^{1.017} \tag{15}$$

$$Sh_L = 0.1672\mathrm{Re}_L^{0.75} Sc_L^{0.75}\left(\frac{\cos(\theta)}{\cos(\pi/4)}\right)^{0.538} \tag{16}$$

$$\frac{a_m}{a_d} = 0.6315\mathrm{Re}_V^{0.0169} We_L^{0.169} Fr_L^{-0.1093} \tag{17}$$

Figure 4 is a parity plot of predicted versus experimental values of the combined column efficiency variable quantity described

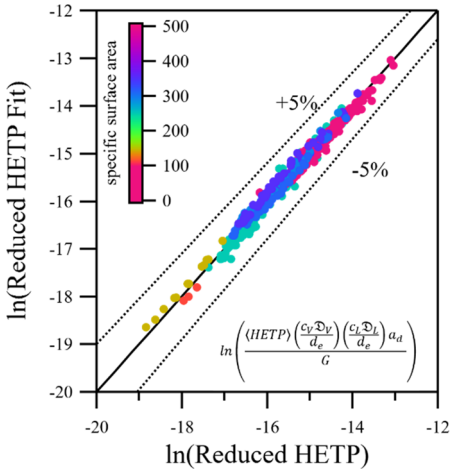


Figure 4. Log scale parity plot of modeled versus measured values of the left-hand side of eq 11 for each total reflux ⟨HETP⟩ data point.

by eq 11. The data have been subcategorized by the dry specific surface area of the packing by coloring the data points accordingly. The data appear to be generally well-described by the suggested correlations above. There is no obvious trend in the way the data points fall with respect to specific surface area. Figure 5 is a similar parity plot of predicted values of $(a_m/a_d)$ to Tsai's measured values. Once again, the data have been


https://doi.org/10.1021/acs.iecr.3c00769
Ind. Eng. Chem. Res. XXXX, XXX, XXX−XXX

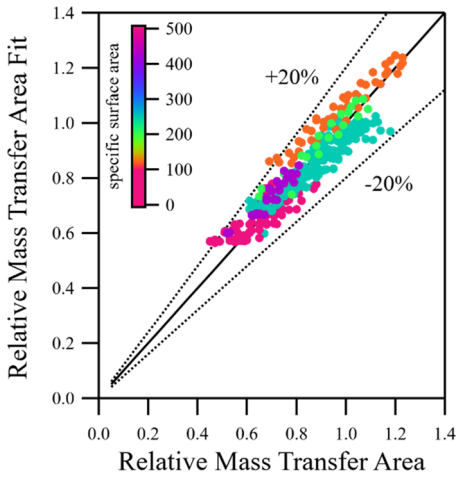


**Figure 5.** Parity plot of modeled mass transfer area ratio versus measured mass transfer area ratio.

subcategorized by coloring the data points to reflect the dry specific surface area of the packing. In this plot, there is a noticeable trend of prediction uncertainty with packing specific surface area. It is clear that the ratio $(a_m/a_d)$ is generally overpredicted for packings with low specific surface areas and underpredicted for packings with higher dry surface areas. We are led to conclude that eq 16 does not fully capture the underlying physics associated surface wettability phenomena and the dependence of these phenomena on the energetic interactions of the liquid film with the packing surface - for example Marangoni effects due to interfacial tension gradients.[36]

## RESULTS

Figures 6, 7, and 8 display tests of effectiveness for eq 15, eq 16, and eq 17 for their ability to reproduce ⟨HETP⟩ values included in our data set. Also included in the plots are predictions of ⟨HETP⟩ from several prominent mass transfer correlations and estimating rules.[11,13,17,19,20]

Additionally, we were interested in testing eq 15 through eq 17 for their ability to predict the performance of packed towers in carbon capture service. Recent economic studies on carbon capture with amine-based solvents almost certainly guarantee that these columns will contain structured packings. Carbon capture pilot plant data from Notz et al. and Gabrielsen et al. were chosen to conduct these tests because each reported enough information to simulate their absorber and/or stripping units.[23,24] Tables 3, 4, 5, 6, 7, and 8 summarize experimental and simulated results important to these experiments, including loadings, weight fractions, and duties. Figures 9 and 10 are comparisons of measured absorber temperatures and calculated profiles for several of the carbon capture experiments of Notz and Gabrielsen. The default Aspen kinetic expressions found in their example simulations for MEA and AMP were used in our analysis. Different sets of

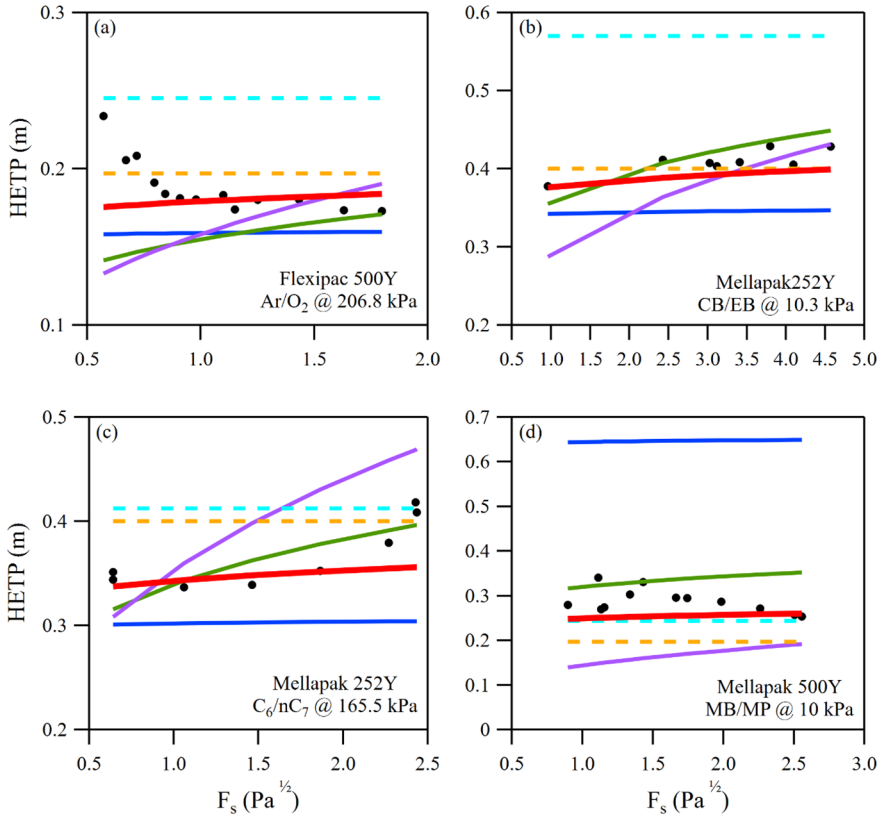


**Figure 6.** (a) ⟨HETP⟩ versus $F_s$ for $Ar/O_2$ separation using Flexipac 500Y at 206.8 kPa.[5] (b) ⟨HETP⟩ versus $F_s$ *for CB/EB separation using Mellapak 252Y at 10.3 kPa.*[4] *(c)* ⟨HETP⟩ *versus* $F_s$ *for cyclo*$C_6$*/n-*$C_7$ *separation using Mellapak 252Y at 165.5 kPa.*[4] *(d)* ⟨HETP⟩ *versus* $F_s$ *for MB/MP separation using Mellapak 500Y at 10 kPa.*[3] *Modeled* ⟨HETP⟩ *as calculated by our correlation is indicated as a solid red line, while the models of Wang et al., Bravo et al., and Hanley and Chen are represented with green, purple, and blue solid lines, respectively.*[17,19,20] *Additionally, estimating rules from Carillo and Harrison and France are indicated by orange and light blue dotted lines.*[11,13]


https://doi.org/10.1021/acs.iecr.3c00769
Ind. Eng. Chem. Res. XXXX, XXX, XXX−XXX

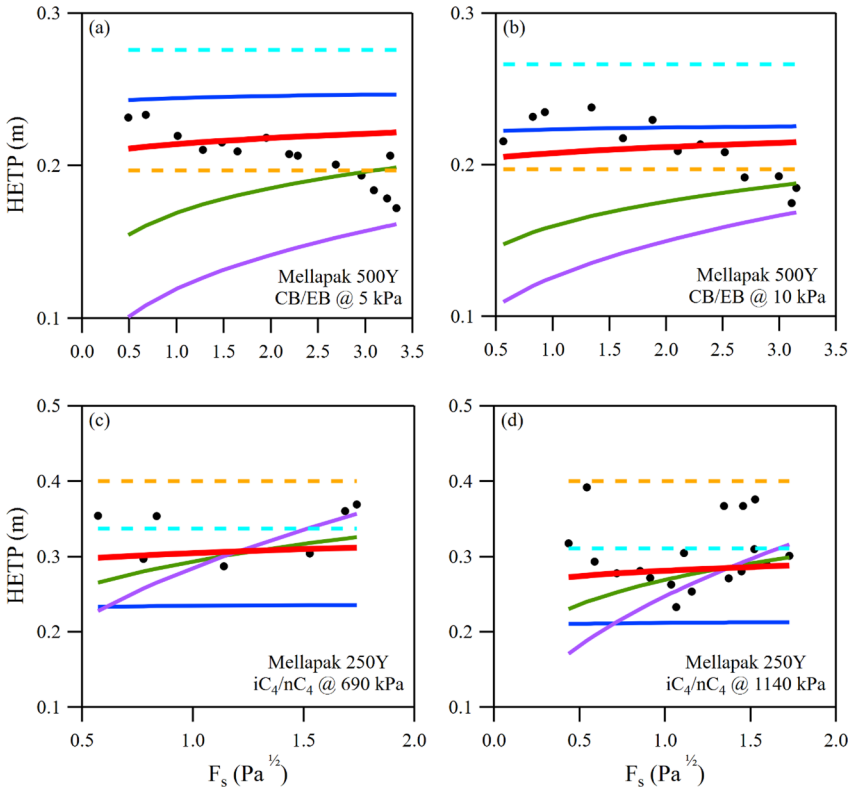


**Figure 7.** (a) ⟨HETP⟩ versus $F_s$ for CB/EB separation using Mellapak 500Y at 5 kPa.[3] (b) ⟨HETP⟩ versus $F_s$ for CB/EB separation using Mellapak 500Y at 10 kPa.[3] (c) ⟨HETP⟩ versus $F_s$ for i-$C_4$/n-$C_4$ separation using Mellapak 250Y at 690 kPa.[1] (d) ⟨HETP⟩ versus $F_s$ for i-$C_4$/n-$C_4$ separation using Mellapak 250Y at 1140 kPa.[1]

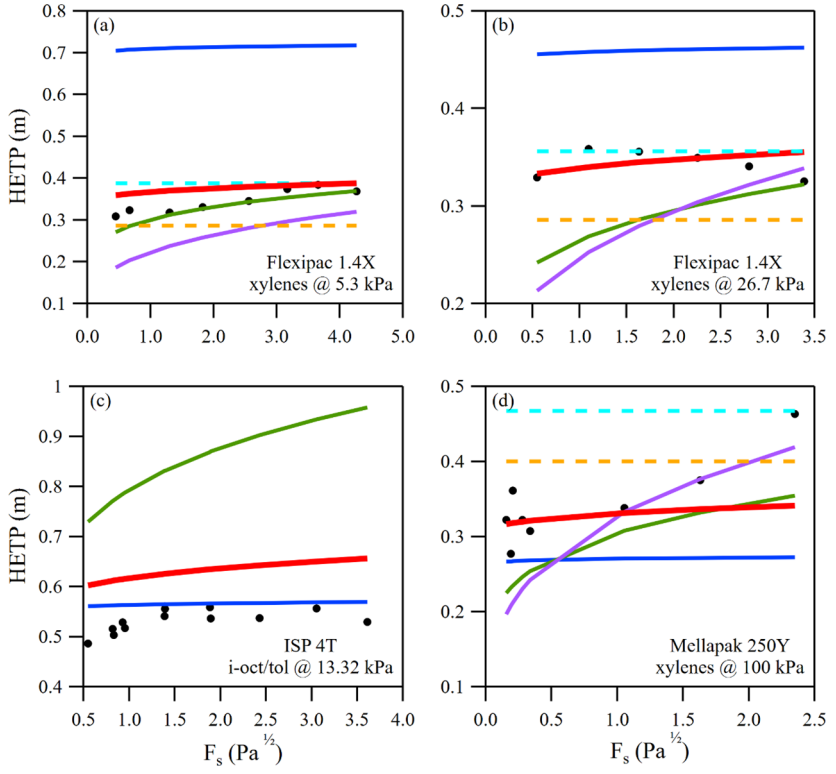


**Figure 8.** (a) ⟨HETP⟩ versus $F_s$ for p-xylene/o-xylene separation using Flexipac 1.4X at 5.3 kPa. (b) ⟨HETP⟩ versus $F_s$ for p-xylene/o-xylene separation using Flexipac 1.4X at 26.7 kPa. (c) ⟨HETP⟩ versus $F_s$ for i-octane/toluene separation using ISP 4T at 13.3 kPa.[7] (d) ⟨HETP⟩ versus $F_s$ for p-xylene/o-xylene separation using Mellapak 250Y at 100 kPa.[1]



https://doi.org/10.1021/acs.iecr.3c00769
Ind. Eng. Chem. Res. XXXX, XXX, XXX−XXX

Table 3. Experimental and Predicted Values Important to the Performance of MEA Absorption/Stripping Gas-Fired Pilot Plant from Notz et al.[23]

| Notz #1 | Experiment | BRF85 | Hanley/ Chen | Wang | This work |
|---|---|---|---|---|---|
| Gas out $\omega_{CO_2}$ | 0.022 | 0.0267 | 0.0183 | 0.0251 | 0.0291 |
| Lean load ($n_{CO_2}/n_{MEA}$) | 0.265 | 0.2222 | 0.2839 | 0.2677 | 0.2645 |
| Rich load ($n_{CO_2}/n_{MEA}$) | 0.386 | 0.3318 | 0.4067 | 0.3813 | 0.3686 |
| $CO_2$ out $\omega_{CO_2}$ | 0.996 | 0.9942 | 0.9942 | 0.9941 | 0.9941 |
| Rich out duty (kW) | 13.524 | 18.046 | 12.900 | 13.119 | 13.068 |
| Lean in $\omega_{H_2O}$ | 0.673 | 0.7695 | 0.6705 | 0.6779 | 0.6717 |
| lean In $\omega_{MEA}$ | 0.275 | 0.1986 | 0.2736 | 0.2700 | 0.2757 |
| Lean in $\omega_{CO_2}$ | 0.052 | 0.0318 | 0.0559 | 0.0521 | 0.0525 |

Table 4. Experimental and Predicted Values Important to the Performance of MEA Absorption/Stripping Coal-Fired Pilot Plant from Notz et al.[23]

| Notz #2 | Experiment | BRF85 | Hanley/ Chen | Wang | This work |
|---|---|---|---|---|---|
| Gas out $\omega_{CO_2}$ | 0.022 | 0.0267 | 0.0183 | 0.0251 | 0.0291 |
| Lean load ($n_{CO_2}/n_{MEA}$) | 0.088 | 0.0750 | 0.0757 | 0.0795 | 0.0816 |
| Rich load ($n_{CO_2}/n_{MEA}$) | 0.308 | 0.2988 | 0.3022 | 0.2926 | 0.2899 |
| $CO_2$ out $\omega_{CO_2}$ | 0.996 | 0.9945 | 0.9945 | 0.9945 | 0.9945 |
| Rich out duty (kW) | 12.4036 | 11.9129 | 11.8712 | 11.9612 | 11.9935 |
| Lean in $\omega_{H_2O}$ | 0.653 | 0.6519 | 0.6514 | 0.6524 | 0.6526 |
| Lean in $\omega_{MEA}$ | 0.284 | 0.2864 | 0.2863 | 0.2871 | 0.2873 |
| Lean in $\omega_{CO_2}$ | 0.063 | 0.0617 | 0.0623 | 0.0605 | 0.0600 |

Table 5. Comparison of the Results from Gabrielsen et al. Gas-Fired AMP Absorption Run 1 with Predictions from Various Mass Transfer Correlations[24]

| Gabrielsen AMP Run 1 | | | | | |
|---|---|---|---|---|---|
| | Experiment | BRF85 | Hanley/ Chen | Wang | This work |
| Gas $CO_2$ bottom (% vol) | 2.62 | 2.62 | 2.62 | 2.62 | 2.62 |
| Gas $CO_2$ top (% vol) | 1.69 | 1.278 | 1.089 | 1.602 | 1.645 |
| $CO_2$ loading top | 0.072 | 0.07201 | 0.07201 | 0.07201 | 0.07201 |
| $CO_2$ loading bottom | 0.178 | 0.224 | 0.2451 | 0.1878 | 0.183 |
| Experimental mass balance error: −0.4% | | | | | |

Table 6. Comparison of the Results from Gabrielsen et al. Gas-Fired AMP Absorption Run 4 with Predictions from Various Mass Transfer Correlations[24]

| Gabrielsen AMP Run 4 | | | | | |
|---|---|---|---|---|---|
| | Experiment | BRF85 | Hanley/ Chen | Wang | This work |
| Gas $CO_2$ bottom (% vol) | 9.28 | 9.28 | 9.28 | 9.28 | 9.28 |
| Gas $CO_2$ top (% vol) | 6.51 | 5.745 | 4.932 | 6.497 | 6.645 |
| $CO_2$ loading top | 0.118 | 0.1181 | 0.1181 | 0.1181 | 0.1181 |
| $CO_2$ loading bottom | 0.379 | 0.4338 | 0.5046 | 0.3678 | 0.3547 |
| Experimental mass balance error: 1.7% | | | | | |

Table 7. Comparison of the Results from Gabrielsen et al. Gas-Fired AMP Absorption Run 7 with Predictions from Various Mass Transfer Correlations[24]

| Gabrielsen AMP Run 7 | | | | | |
|---|---|---|---|---|---|
| | Experiment | BRF85 | Hanley/ Chen | Wang | This work |
| Gas $CO_2$ bottom (% vol) | 12.96 | 12.96 | 12.96 | 12.96 | 12.96 |
| Gas $CO_2$ top (% vol) | 9.83 | 9.898 | 9.682 | 7.405 | 8.692 |
| $CO_2$ loading top | 0.17 | 0.17 | 0.17 | 0.17 | 0.17 |
| $CO_2$ loading bottom | 0.459 | 0.4385 | 0.4571 | 0.6522 | 0.5423 |
| Experimental mass balance error: 4.9% | | | | | |

Table 8. Comparison of the Results from Gabrielsen et al. Gas-Fired AMP Absorption Run 11 with Predictions from Various Mass Transfer Correlations[24]

| Gabrielsen AMP Run 11 | | | | | |
|---|---|---|---|---|---|
| | Experiment | BRF85 | Hanley/ Chen | Wang | This work |
| Gas $CO_2$ bottom (% vol) | 10.27 | 10.27 | 10.27 | 10.27 | 10.27 |
| Gas $CO_2$ top (% vol) | 8.01 | 7.108 | 6.474 | 7.797 | 8.048 |
| $CO_2$ loading top | 0.284 | 0.284 | 0.284 | 0.284 | 0.284 |
| $CO_2$ loading bottom | 0.4 | 0.438 | 0.4663 | 0.4057 | 0.3945 |
| Experimental mass balance error: −0.9% | | | | | |

kinetic parameters and reaction stoichiometries would most likely affect agreement with experimental data to some degree.

Interestingly, the values of power law exponents $C_2$ and $C_3$ were ultimately set to unity, which causes eq 13 to apply for the final version of our correlation. Replacing $k_y$ in eq 7 with eq 13 leads to a cancellation of the molar flux in the vapor phase contribution to ⟨HETP⟩. The final vapor phase resistance contribution to the ⟨HETP⟩ is thus

$$\left(C_1\left(\frac{\cos(\theta)}{\cos(\pi/4)}\right)^{C_4}\right)^{-1}$$

which is only a function of channel inclination angle. The same fortuitous cancellation of all thermodynamic and transport properties does not occur on the liquid side since the power law exponents $C_6$ and $C_7$ are 0.75 in the final version of our correlations. This means $k_x$ remains weakly dependent on property related effects. Nevertheless, if we were to assume that eq 14 could approximately represent the relationship between $k_x$ and the liquid molar flux, then the liquid side resistance would also become a function of inclination angle


https://doi.org/10.1021/acs.iecr.3c00769
Ind. Eng. Chem. Res. XXXX, XXX, XXX−XXX

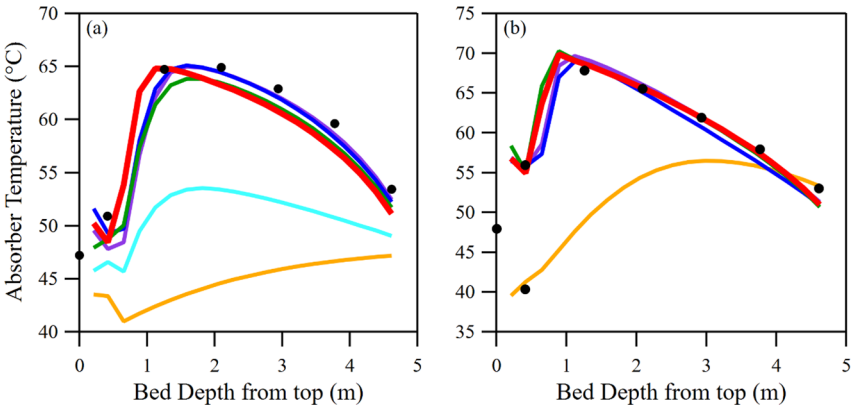


**Figure 9.** (a) and (b) display absorber temperature versus bed depth used in carbon capture pilot plant experiments 1 and 2 of Notz et al.[23] Modeled absorber temperature as calculated by our correlation is indicated as a solid red line, while the models of Wang et al., Bravo et al. 1985, Bravo et al. 1992, Hanley and Chen, and Billet and Schultes are represented with green, purple, orange, blue, and light blue solid lines, respectively.[17−20,38]

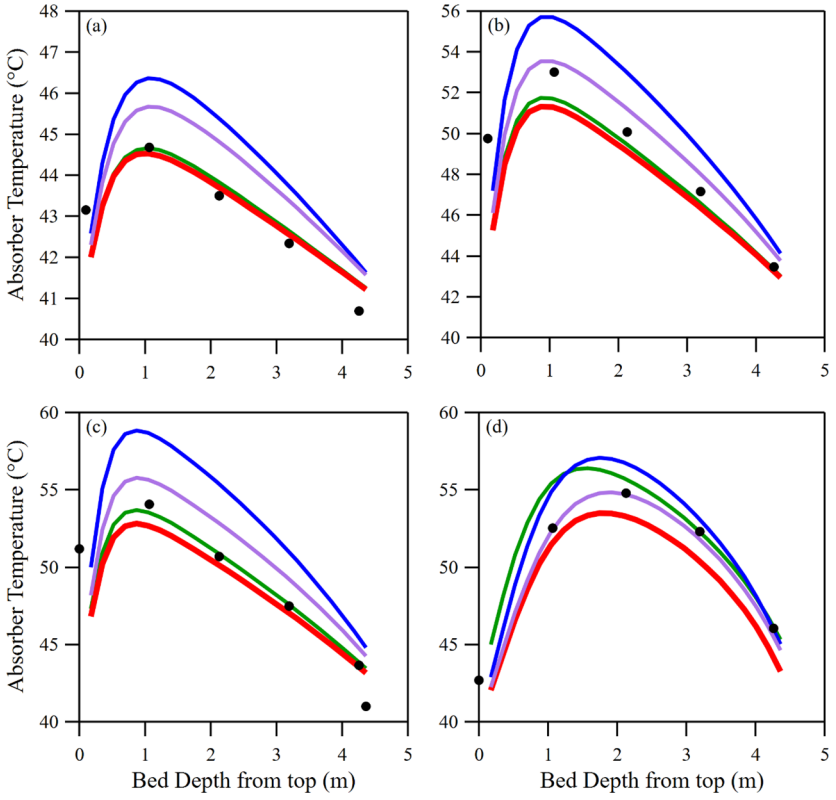


**Figure 10.** (a), (b), (c), and (d) display absorber temperature versus bed depth used in carbon capture pilot plant experiments R1, R4, R7, and R11 of Gabrielsen et al.[24]

alone. We determined the effective values for the liquid side resistances for "Y" and "X" style packings by performing linear regressions of $k_x$ against liquid molar flux for each angle. As a final step, we replaced the mass transfer area term in the denominator of eq 7 with the average value of $(a_m/a_d)$ multiplied by $a_d$. Eq 18 and eq 19 show the results for new "Y" and "X" style estimating rules based on the above simplifications.

$$\langle \mathrm{HETP}_Y \rangle \cong \frac{\left(\frac{1}{0.0478} + \frac{1}{0.0156}\right)}{0.7997 a_d} \cong \frac{106}{a_d} \tag{18}$$

$$\mathrm{HETP}_X \cong \frac{\left(\frac{1}{0.0333} + \frac{1}{0.0145}\right)}{0.7997 a_d} \cong \frac{123}{a_d} \tag{19}$$

Surprisingly, eq 18 for "Y" style packings is in excellent agreement with the well-known estimating rule $100/a_d$ reported by Harrison and France.[11] Eq 19 is, we believe, a unique rule-of-thumb for "X" style packings. Figure 11 compares predictions of eq 18 and eq 19 to vendor-recommended ⟨HETP⟩ values.



https://doi.org/10.1021/acs.iecr.3c00769
Ind. Eng. Chem. Res. XXXX, XXX, XXX−XXX

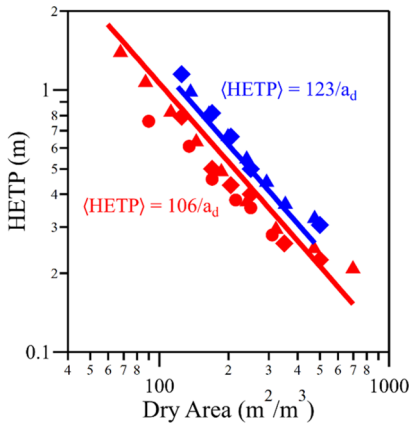


**Figure 11.** Comparison of predictions from eq 18 and eq 19 to vendor-recommended ⟨HETP⟩ values as a function of dry packing specific surface area, $a_d$. Koch-Glitsch Flexipac, Koch-Glitsch ISP, and Sulzer Mellapak data are represented by triangles, circles, and diamonds, respectively. Red signifies "Y" style packings and predictions, while those in blue signify "X" styles.

## CONCLUSIONS

The performance of eq 15 through eq 17 in simulations of mass transfer in distillation and for absorption/stripping represents an advance over other available correlations for structured packings. Figure 2 and Figure 12 present ⟨HETP⟩

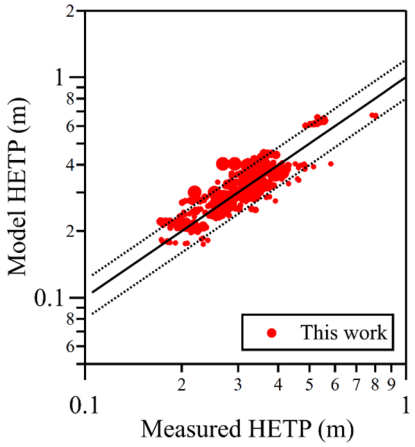


**Figure 12.** ⟨HETP⟩ parity plot for the mass transfer correlation developed by the authors. Dotted lines are ±20% around the diagonal.

parity plots for a number of the mass transfer correlations examined in this paper. The correlation presented in this paper noticeably outperforms the others which are displayed. While the power law forms used in this paper cannot adequately capture the true complexity of these types of unit operations, we have shown that they do remarkably well for a much-expanded range of column operating conditions and fluid transport and thermodynamic properties away from flood for both distillation operations as well as for carbon capture.

However, much work remains before a complete model of mass transfer in structured packings can be claimed. For example, the efficiency data for i-$C_4$/n-$C_4$ taken at 2.76 MPa by FRI remains enigmatic, as no correlation examined/reported on in this paper is able to even come close to the magnitudes of the reported ⟨HETP⟩s for the experimental range of $F_s$ values.[1] In addition, the simplicity of form for all of these correlations cannot possibly capture the complex behavior observed, such as the notorious "hump" seen at intermediate $F_s$. Figure 13 displays the poor performance of our correlation

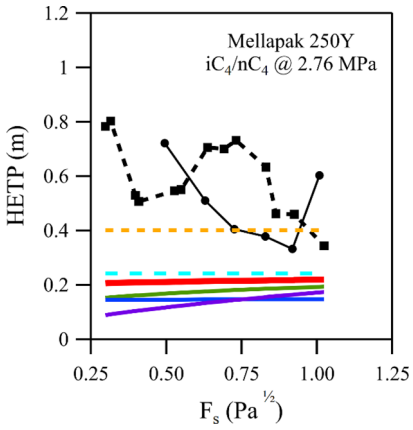


**Figure 13.** ⟨HETP⟩ versus $F_s$ for i-$C_4$/n-$C_4$ separation using Mellapak 250Y at 27.6 MPa.[1]

and others for this particular experiment. It should be noted that efficiency models have been proposed that capture this type of behavior.[37] Unfortunately, the complexity of the proposed equations coupled with the paucity and quality of the experimental data puts effective use of these equations out of reach.

## ASSOCIATED CONTENT

### Supporting Information

The Supporting Information is available free of charge at https://pubs.acs.org/doi/10.1021/acs.iecr.3c00769.

Additional graphical and tabular results and comparisons (PDF)

## AUTHOR INFORMATION

### Corresponding Author

**Brian F. Hanley** − *Cain Department of Chemical Engineering, Louisiana State University, Baton Rouge, Louisiana 70803, United States;* orcid.org/0000-0001-5142-3597; Email: brianhanley@lsu.edu

### Author

**Jack Wilfert** − *Cain Department of Chemical Engineering, Louisiana State University, Baton Rouge, Louisiana 70803, United States*

Complete contact information is available at: https://pubs.acs.org/10.1021/acs.iecr.3c00769

### Funding

No external funding was used in the preparation of this manuscript. Louisiana State University has paid the open access fee for this document through a transformative agreement with the American Chemical Society.

### Notes

The authors declare no competing financial interest.

## SYMBOLS

$a_d$: dry packing surface area per unit volume
$a_m$: mass transfer surface area per unit volume
$c_L$: molar concentration of the liquid phase



https://doi.org/10.1021/acs.iecr.3c00769
Ind. Eng. Chem. Res. XXXX, XXX, XXX−XXX

$c_V$: molar concentration of the vapor phase
$C_i$: fitting constant
$C_x$: composition dependent correction factor used to convert the point HETP to an average HETP
$C_y$: composition dependent correction factor used to convert the point HETP to an average HETP
$D_{ij}^{\circ}$: tracer diffusivity of component $i$ in liquid $j$
$\mathcal{D}_V$: vapor phase binary diffusion coefficient
$\mathcal{D}_L$: liquid phase binary diffusion coefficient
$d_e$: packing equivalent diameter $-4\varepsilon/a_d$
$Fr_L$: liquid phase Froude number - $\frac{v_L^2}{gd_e}$
$F_S$: superficial F-factor - $v_V\sqrt{\rho_V}$
$G$: vapor molar flux
HETP: height equivalent to a theoretical plate; usually the point HETP
⟨HETP⟩: average HETP over the column height as compared to the point HETP
$k_x$: liquid side mass transfer coefficient based on mole fraction driving forces
$k_y$: vapor side mass transfer coefficient based on mole fraction driving forces
$m$: slope of vapor−liquid equilibrium curve
$Re_L$: liquid phase Reynolds number
$Re_V$: vapor phase Reynolds number
$Sc_L$: liquid phase Schmidt number − $\frac{\mu_L}{\rho_L\mathcal{D}_L}$
$Sc_V$: vapor phase Schmidt number − $\frac{\mu_V}{\rho_V\mathcal{D}_V}$
$Sh_L$: liquid phase Sherwood number − $\frac{k_x d_e}{c_L\mathcal{D}_L}$
$Sh_V$: vapor phase Sherwood number − $\frac{k_y d_e}{c_V\mathcal{D}_V}$
$v_L$: liquid velocity based on the total cross-sectional area of the column
$v_V$: vapor velocity based on the total cross-sectional area of the column
$We_L$: liquid phase Weber number − $\frac{\rho_L d_e v_L^2}{\sigma_L}$
$x$: liquid phase mole fraction of the more volatile component
$y$: vapor phase mole fraction of the more volatile component

## GREEK LETTERS

$\alpha$: relative volatility
$\beta$: thermodynamic correction for solution nonideality
$\varepsilon$: packing void fraction
$\theta$: packing inclination angle measured from the horizontal
$\mu_L$: liquid dynamic viscosity
$\mu_V$: vapor dynamic viscosity
$\rho_L$: liquid mass density
$\rho_V$: vapor mass density
$\sigma_L$: interfacial tension

## REFERENCES


(1) Fitz, C.; Kunesh, J. G.; Shariat, A. Performance of Structured Packing in a Commercial-Scale Column at Pressures of 0.02−27.6 bar. *Ind. Eng. Chem. Res.* **1999**, *38*, 512−518.
(2) Gualito, J. J.; Cerino, F. J.; Cardenas, J. C.; Rocha, J. A. Design Method for Distillation Columns Filled with Metallic, Ceramic, or Plastic Structured Packings. *Ind. Eng. Chem. Res.* **1997**, *36* (5), 1747−1757.
(3) Bradtmöller, C.; Scholl, S. Geometry and Viscosity Effects on Separation Efficiency in Distillation. *Chem. Eng. Res. Des.* **2015**, *99*, 75−86.
(4) Bennett, K.; Pilling, M. Efficiency Benefits of High Performance Structured Packings. In *Department of Energy Texas Technology Showcase, D2: Separations or Distillation Technologies*; Houston, 2003.
(5) Bennett, D. L.; Ludwig, K. A.; Witmer, G. S.; Woods, C. M. Separating Argon/Oxygen Mixtures Using a Structured Packing. US4836836A, June 1989.
(6) Olujić, Ž.; Rietfort, T.; Jansen, H.; Kaibel, B.; Zich, E.; Frey, G.; Ruffert, G.; Zielke, T. Experimental Characterization and Modeling of High Performance Structured Packings. *Ind. Eng. Chem. Res.* **2012**, *51* (11), 4414−4423.
(7) Koshy, T. D.; Rukovena, F. Distillation Pilot Plant Design, Operating Parameters, and Scale-Up Considerations. Presented at The Chemical Engineers' Resource Page. https://kipdf.com/distillation-pilot-plant-design-operating-parameters-and-scale-up-considerations_5aadf8fb1723dddd48227b0b.html (accessed 2023-05-10).
(8) Kister, H. Z. *Distillation Design*; McGraw-Hill Education: 1992.
(9) Tsai, R. E. *Mass Transfer Area of Structured Packing*; University of Texas: Austin, TX, 2010.
(10) Wilfert, J.; Hanley, B. Progress Towards a Comprehensive Model for Mass Transfer in Structured Packings. https://www.aiche.org/academy/conferences/aiche-spring-meeting-and-global-congress-on-process-safety/2022/proceeding/paper/156e-progress-towards-comprehensive-model-mass-transfer-and-hydraulics-structured-packings (accessed 2023-05-10).
(11) Harrison, M. E. Distillation Column Troubleshooting. Part 2. Packed Column. *Chem. Eng.* **1989**, *96*, 121.
(12) Lockett, M. J. Easily Predict Structured-Packing HETP. *Chemical Engineering Progress*;American Institute of Chemical Engineers: New York, January 1998; Vol. *94*, p 60.
(13) Carillo, F.; Martín, A.; Roselló, A. A Shortcut Method for the Estimation of Structured Packings HEPT in Distillation. *Chem. Eng. Technol.* **2000**, *23* (5), 425−428.
(14) Wang, G. Q.; Yuan, X. G.; Yu, K. T. Review of Mass-Transfer Correlations for Packed Columns. *Ind. Eng. Chem. Res.* **2005**, *44* (23), 8715−8729.
(15) Čmelíková, T.; Valenz, L.; Lyko Vachková, E.; Rejl, F. J. Basic Separation Efficiency and Hydraulic Data of MellapakPlus 452.Y Structured Packing under Distillation Conditions. *Chem. Eng. Res. Des.* **2021**, *172*, 175−185.
(16) Chilton, T. H.; Colburn, A. P. Mass Transfer (Absorption) Coefficients Prediction from Data on Heat Transfer and Fluid Friction. *Ind. Eng. Chem.* **1934**, *26* (11), 1183−1187.
(17) Bravo, J. L.; Rocha, J.; Fair, J. R. Mass Transfer in Gauze Packings. *Hydrocarb. Process.* **1985**, *64* (1), 91−95.
(18) Billet, R.; Schultes, M. Prediction of Mass Transfer Columns with Dumped and Arranged Packings: Updated Summary of the Calculation Method of Billet and Schultes. *Chem. Eng. Res. Des.* **1999**, *77* (6), 498−504.
(19) Hanley, B.; Chen, C. C. New Mass-Transfer Correlations for Packed Towers. *AIChE J.* **2012**, *58* (1), 132−152.
(20) Wang, C.; Song, D.; Seibert, F. A.; Rochelle, G. T. Dimensionless Models for Predicting the Effective Area, Liquid-Film, and Gas-Film Mass-Transfer Coefficients of Packing. *Ind. Eng. Chem. Res.* **2016**, *55* (18), 5373−5384.
(21) Maćkowiak, J. Prediction of Separation Efficiency of Structured and Stacked Packings under Low and Normal Pressure. *Chem. Eng. Res. Des.* **2022**, *186*, 713−729.
(22) Olujić, Ž.; Behrens, M.; Colli, L.; Paglianti, A. Predicting the Efficiency of Corrugated Sheet Structured Packings with Large Specific Surface Area. *Chem. Biochem. Eng. Q.* **2004**, *18* (2), 89−96.
(23) Notz, R.; Mangalapally, H. P.; Hasse, H. Post Combustion CO2 Capture by Reactive Absorption: Pilot Plant Description and Results of Systematic Studies with MEA. *Int. J. Greenh. Gas Control* **2012**, *6*, 84−112.



https://doi.org/10.1021/acs.iecr.3c00769
Ind. Eng. Chem. Res. XXXX, XXX, XXX−XXX

(24) Gabrielsen, J.; Svendsen, H. F.; Michelsen, M. L.; Stenby, E. H.; Kontogeorgis, G. M. Experimental Validation of a Rate-Based Model for CO2 Capture Using an AMP Solution. *Chem. Eng. Sci.* **2007**, *62* (9), 2397−2413.
(25) Bishnoi, S.; Rochelle, G. T. Absorption of Carbon Dioxide in Aqueous Piperazine/Methyldiethanolamine. *AIChE J.* **2002**, *48* (12), 2788−2799.
(26) Chen, E. *Carbon Dioxide Absorption into Piperazine Promoted Potassium Carbonate Using Structured Packing*; The University of Texas at Austin: Texas, United States, 2007.
(27) Kays, W. M.; London, A. L. *Compact Heat Exchangers*, 3rd ed.; McGraw-Hill: New York, 1984.
(28) Wakao, N.; Kagei, S. *Heat and Mass Transfer in Packed Beds*; Taylor & Francis: 1982; Vol. *1*.
(29) Hsiung, T. H.; Thodos, G. Mass-Transfer Factors from Actual Driving Forces for the Flow of Gases through Packed Beds (0.1 < Re < 100). *Int. J. Heat Mass Transfer* **1977**, *20* (4), 331−340.
(30) Aspen Technology, I. Is It Possible to Use Correlations Other than the Built-in Ones in Rate-Based Distillation? *Aspen Knowledge Base Article 000095148*; Aspen Technology, Inc. https://esupport.aspentech.com/S_Article?id=000095148, (accessed 2023-02-18).
(31) Rejl, F. J.; Haidl, J.; Valenz, L.; Marchi, A.; Moucha, T.; Petříček, R.; Brunazzi, E. Liquid-Phase Mass-Transfer Coefficients of Mellapak Structured Packings under Desorption of Oxygen from Primary Alcohols. *Chem. Eng. Res. Des.* **2017**, *127*, 1−9.
(32) Valenz, L.; Rejl, F. J.; Šíma, J.; Linek, V. Absorption Mass-Transfer Characteristics of Mellapak Packings Series. *Ind. Eng. Chem. Res.* **2011**, *50* (21), 12134−12142.
(33) NIST Reference Fluid Thermodynamic and Transport Properties Database (REFPROP): Version 10. https://www.nist.gov/srd/refprop (accessed 2023-02-18).
(34) Vignes, A. Diffusion in Binary Solutions. Variation of Diffusion Coefficient with Composition. *Ind. Eng. Chem. Fundam.* **1966**, *5* (2), 189−199.
(35) Wavemetrics website. https://www.wavemetrics.com/ (accessed 2021-11-15).
(36) Proctor, S. J.; Biddulph, M. W.; Krishnamurthy, K. R. Effects of Marangoni Surface Tension Forces on Modern Distillation Packings. *AIChE J.* **1998**, *44* (4), 831−835.
(37) Hanley, B.; Dunbobbin, B.; Bennett, D. A Unified Model for Countercurrent Vapor/Liquid Packed Columns. 2. Equations for the Mass-Transfer Coefficients, Mass-Transfer Area, the HETP, and the Dynamic Liquid Holdup. *Ind. Eng. Chem. Res.* **1994**, *33*, 1222.
(38) Bravo, J.; Rocha, J.; Fair, J. A Comprehensive Model for the Performance of Columns Containing Structured Packings. In *IChemE Symposium Series No. 128*; 1992.


https://doi.org/10.1021/acs.iecr.3c00769
*Ind. Eng. Chem. Res.* XXXX, XXX, XXX−XXX